Books of Abstracts

Résumés

CANM 2023 Annual Scientific Meeting, Brookstreet Hotel, Ottawa
Réunion annuelle scientifique de l'ACMN 2023, Hotel Brookstreet, Ottawa

October 19th to the 21st
Du 19 au 21 octobre

001- **Lawrence Raymond V. Mariano**

Sentinel Lymph Node Localization in Filipino Breast Cancer Patients Using Blue Dye with or without Lymphoscintigraphy: A Single-Center Retrospective Analysis

Primary Investigator:
Lawrence Raymond V. Mariano, MD

Co-Investigators:
Eddie A. Lim, MD, MBAH, FPSNM
Nicole Patricia A. Hui, MD, DPSBNM

Department of Nuclear Medicine and PET/CT Center
The Medical City Ortigas

ABSTRACT

BACKGROUND: Sentinel lymph node (SLN) localization has long been utilized in the management of breast cancer patients who are to undergo surgical intervention. The use of blue dye alone or in combination with lymphoscintigraphy has been the subject of much research, aimed to establish the best possible standard of care for early management and prognostication of breast disease. This study aimed to compare the sensitivity, specificity, detection accuracy, and false negative rates of these two techniques.

METHODS: Patient records from 2018-2022 were included in the study. Data from 350 female patients, of whom 167 underwent blue dye localization and 183 underwent both blue dye and lymphoscintigraphy, were analyzed through a comparative chi-square analysis.

RESULTS: Analysis revealed a significantly higher detection accuracy and sensitivity, as well as lower false negative rates ($p<0.001$) for the combination technique in all patients, as well as in patients with previous excision biopsy of the breast. Specificity of the two groups, however, were comparable and not statistically different ($p=0.93$). These results are concordant with previous literature in terms of sensitivity and false negative rates, and also provide novel data regarding higher detection accuracy.

CONCLUSION: The combination of lymphoscintigraphy and blue dye in the localization of SLNs may become the standard of care for early breast cancer patients in need of surgery, regardless of treatment history, as it showed significantly higher detection accuracy and sensitivity, and lower false negative rates than utilizing blue dye alone.

002- **Debra Dawson**

Background:

Prostate Specific Membrane Antigen (PSMA)-based diagnostics and therapeutics are proving valuable in identifying disease and providing targeted radioligand therapy (RLT) for disseminated disease in prostate cancer (PC). With such successful integration of these tools in limited PC presentations, there is a real need for trials testing PSMA-based approaches more broadly.

Objectives/Methods:

We review the ongoing trials registered on ClinicalTrials.gov which aim to evaluate PSMA-PET or PSMA-RLT applications. We outline clinical contexts which have significant study and therefore may see imminent change, as well as contexts which are lacking in study in the hopes of guiding future research.

Results:

There are promising Phase 3 trials looking at how PSMA-PET can augment radiotherapeutic or surgical planning. Head-to head trials are ongoing comparing PSMA radioligands or PSMA-PET to other imaging modalities. Other studies are looking at the use of PSMA-PET in follow up to assess response to treatment/disease progression. Diagnostic trials outside of prostate cancer conditions are few, with the most prominent presence being in HCC, or solid cancers as a group. In the PSMA-based therapeutic domain, important trials will be leading the way to implementing PSMA-RLT in earlier phases of PC (before mCRPC). Other trials will provide clarifications as to the relative efficacies of 177Lu-PSMA-617 and abiraterone or enzalutamide ARSI therapies.

Conclusions:

Standardized reporting guidelines for PSMA-PET “PSMAomics” are expected to evolve (including in follow-up). We expect that PSMA-PET will become fundamental in the work-up of patients before targeted radiotherapy or surgery. Trials examining intensification strategies through targeted radiotherapy, combination systemic therapies, and RLTs have the potential to demonstrate improved clinical outcomes. The results of ongoing trials will likely clarify the benefits of PMSA-PET and PSMA-RLT in metastatic PC including in oligometastatic and hormone-sensitive disease, however, there is a sparsity of trials evaluating PSMA-RLT outside of metastatic castrate-resistant prostate cancer.

003 – **Dominic Alcantara**

A retrospective study on the utility of semi-quantitative analysis in parathyroid scintigraphy

Dominic Alcantara[1]*, Nicole Patricia Hui[1], Eddie Lim[1]
[1]Nuclear Medicine and PET-CT Center, The Medical City, Ortigas, Philippines
*Email address of corresponding author: alcantaradomz@gmail.com

ABSTRACT:

Objectives
Lesion-to-background ratios (LBR) thresholds, a mathematical value of a lesion's radiation counts divided by the background counts, have not been established yet in the Philippines likely due to limited studies on preoperative parathyroid scintigraphy. To evaluate their utility, early and delayed LBRs were compared to surgical histopathology, parathyroid gland volume, ionized calcium, and intact parathyroid hormone (PTH).

Methods
A retrospective chart review was done on hyperparathyroidism patients in a tertiary hospital who underwent dual phase Technetium-99m sestamibi parathyroid scintigraphy with corresponding parathyroidectomy from January 2017 to June 2023, leading to analysis of thirty patient records.

Results
Surgical histopathology assessments were predominantly parathyroid adenoma (83.3%), two parathyroid hyperplasia (6.7%), one benign parathyroid (3.3%), and two nodular thyroid hyperplasia (6.7%). The dual phase parathyroid scan is concordant with surgical histopathology, exhibiting a sensitivity of 96.3%, specificity of 66.7%, and positive predictive value (PPV) of 96.3%. Through area under the curve analysis, early LBR of 3.7 and delayed LBR of 2.2 showed similar PPV (94.4% and 95.5%). Additionally, Spearman correlation analysis showed early and delayed LBR having a moderate correlation with parathyroid gland volume (ρ = 0.68 and 0.64), and fair correlation with ionized calcium (ρ = 0.31 and 0.50) & intact PTH (ρ = 0.45 and 0.48).

Conclusions
The results of this single-center retrospective study demonstrated a significant relationship between LBR and hyperplastic parathyroid. Use of LBR may lead to improvements in diagnostic accuracy as an adjunct parameter in parathyroid scan interpretation.

Keywords: *hyperparathyroidism, parathyroid scan, sestamibi, parathyroidectomy*

004- **Carl Joshua Chianpian**

Complete and Sustained Response After Peptide Receptor Radionuclide Therapy in a 66-Yea rOld Filipino Male with Metastatic Pancreatic Neuroendocrine Tumor: A Case Report

Primary Author: Carl Joshua M. Chianpian, MD Co-Authors: Patricia A. Bautista-Peñalosa, MD Carl Johnry J. Santos, MD Irene S. Bandong, MD St. Luke's Medical Center, Quezon City, Philippines Department of Nuclear Medicine and Theranostics

ABSTRACT

The introduction of peptide receptor radionuclide therapy (PRRT) to the Philippines has allowed for novel approaches in the management of neuroendocrine tumors (NETs). This case report details the management of a 66-year-old Filipino man diagnosed with metastatic pancreatic NET after biopsy and staging with Ga-68 DOTATATE PET-CT. After poor response to somatostatin analogue therapy, the patient was advised to undergo PRRT. Upon completing four cycles of PRRT with Lu-177 DOTATATE, the metastatic hepatic lesions showed resolution and the pancreatic tail tumor exhibited regression, allowing the patient to undergo surgical resection of the primary tumor. On follow-up, he is declared to be in remission with good quality of life and no imaging evidence of recurrence. The case underscores the diagnostic and therapeutic utility of radiolabeled somatostatin analogues along with the importance of a multidisciplinary approach in the management of an initially unresectable metastatic pancreatic NET.

Key words: peptide receptor radionuclide therapy, metastatic pancreatic neuroendocrine tumor, Ga-68 DOTATATE, Lu-177 DOTATATE, Philippines

005- **Mary Amie Gelina E. Dumatol**

Early versus Delayed Post-Therapy Whole Body Scintigraphy for Well-Differentiated Thyroid Carcinoma: a Meta-Analysis

Mary Amie Gelina E. Dumatol, MD[1]

Jessica Elise A. Kuizon, MD[1]

Michele D. Ogbac, MD[1]

[1]Nuclear Medicine Division, Philippine Heart Center, Philippines

ABSTRACT

Background: No clear consensus exists as to the optimal timing for conducting whole body scintigraphy (WBS) after radioactive iodine (RAI) therapy for differentiated thyroid carcinoma. This study aimed to compare the utility of early versus delayed post-therapy WBS in identifying residual lesions and metastases.

Methods: A systematic review of existing literature was done, yielding 6 observational studies relevant to the subject. Meta-analyses were done comparing lesion detecting rates of early (3-4 days post-RAI) and delayed (7-11 days post-RAI) post-therapy WBS for thyroid remnants and metastases in the lymph nodes, lungs, and bone using a random-effects model with odds ratios (OR) and 95% confidence intervals (CIs). A subgroup analysis was also done relating to the type of collimator used in imaging.

Results: There was no evidence to support that conducting WBS at either an early or delayed time after RAI therapy is superior to the other in detecting thyroid remnants (OR 1.11; 95% CI 0.86 – 1.42; $p = 0.42$), nodal (OR 1.01; 95% CI 0.74 – 1.38; $p = 0.97$), lung (OR 0.79; 95% CI 0.55 – 1.13; $p = 0.20$), and bone (OR 0.89; 95% CI 0.56 – 1.43; $p = 0.64$) metastases.

Conclusion: There is no significant difference between early and delayed post-therapy whole body scintigraphy in terms of detecting thyroid remnants and nodal, lung, and bone metastases in patients with well-differentiated thyroid carcinoma.

Keywords: post-therapy whole body scintigraphy (WBS), Iodine-131 (I-131), radioactive iodine (RAI) therapy, thyroid cancer

006- **Dr. Sandor Demeter**

Evolving radiation protection regulations and guidelines – what does it mean for Nuclear Medicine

I can contest that after serving two terms as an ICRP committee member (C3-Protection in Medicine), as well as two terms as a CNSC regulator, the pace of change in radiation protection guidelines has been slow, if not glacial. However, recently there have been significant updates to radiation protection standards and dose limits which can influence how compliance is demonstrated to the Canadian nuclear regulator – the CNSC. At the same time there have been significant advances in the licensing of new diagnostic and therapeutic radiopharmaceuticals which will increase nuclear-medicine's profile as well as present more novel radiation protection scenarios. This session will tease out changes that are most applicable to nuclear medicine settings and will reflect recent changes to CNSC's Radiation Protection regulations as well as what has been percolating at the ICRP. These issues include: a more existential discussion on getting rid of equivalent dose and sticking with straight organ dose (Gy) and effective dose (Sv), changes to dose limits for lens of eye, no longer requiring NEWs to declare pregnancy, an increased interest in the ethics of radiation protection and seeking a new model for assessing the economic impact of ALARA in medical settings. The LNT model continues to be controversial with very polarized opinions, for and against, its validity – is there a pragmatic middle ground? Perhaps – the CNSC's position on LNT will be discussed.

007- **Yousif Al-Ali**

Flashy Lungs and Sarcoidosis: Not Always a Sign of Disease Activity

Yousif A. Lucinian[a], MD PharmD, Patrick Martineau[b,c], MD PhD, Francois Harel[a], MD PhD, Matthieu Pelletier-Galarneau, MD MSc[a]

[a] Department of Medical Imaging, Institut de Cardiologie de Montréal, Montréal, Québec, Canada

[b] BC Cancer, Vancouver, British Columbia, Canada

[c]Department of Radiology, University of British Columbia, Vancouver, British Columbia, Canada

Yousif A. Lucinian MD PharmD : yousif.al-ali@umontreal.ca

Patrick Martineau MD PhD : patrick.martineau@bccancer.bc.ca

Francois Harel MD PhD : francois.harel@icm-mhi.org

Matthieu Pelletier-Galarneau MD MSc : matthieu.pelletier-galarneau@icm-mhi.org

Conflict of interest: All authors declare the absence of conflicts of interest.

Introduction

Methotrexate (MTX) lung toxicity can result in pneumonitis, which typically presents as progressive dyspnea, cough, and fever. As prognosis is excellent with appropriate clinical management, it is important to recognize methotrexate-induced pneumonitis (MtxIP), especially in patients treated for sarcoidosis. In the presence of known sarcoidosis, new fluorodeoxyglucose (FDG) lung uptake is not necessarily related to pulmonary sarcoidosis (PS).

We herein describe the first case of MtxIP documented by FDG positron emission tomography (PET)/computed tomography (CT).

Case report

A 68-year-old man presented with shortness of breath and syncope. Rhythm strips revealed advanced atrioventricular block (Figure 1.A). Despite being limited by breathing artefact, cardiovascular magnetic resonance (Figure 1.B) showed subendocardial late gadolinium enhancement within the basal interventricular septum and laterobasal wall in a pattern compatible with an ischemic etiology. Epicardial fat infiltration was absent. As coronary angiography only showed minimal non-obstructive coronary artery disease, an alternative diagnosis such as CS was suspected.

Whole body FDG-PET/CT (Figure 2.A) was performed following a myocardial suppression protocol to exclude CS. Pathological FDG uptake (SUVmax=15.4) was noted within the myocardium (Figure 2.B) involving the left ventricular free wall and septal wall. Increased uptake (SUVmax=14.9) was present within multiple intrathoracic lymph nodes (LN) (Figure 2.C). Lung parenchymal involvement was absent. Hilar LN biopsy confirmed the presence of non-caseating granulomas, compatible with sarcoidosis. A clinical diagnosis of CS based on the modified Japanese Circulation Society criteria and the Heart Rhythm Society criteria was retained with extra-cardiac involvement of intrathoracic LN (1,2). A pacemaker was implanted, and treatment was initiated with oral prednisone 50 mg once per day and oral MTX 20 mg once a week.

The patient's shortness of breath resolved and syncope did not recur. A follow-up FDG-PET/CT (Figure 3.A) was performed after three months of treatment. Overall, there was complete resolution of pathological FDG uptake within both the myocardium (Figure 3.B) and intrathoracic LN (Figure 3.C). Treatment regimen was maintained without modification.

Three months later, the patient was hospitalized for new onset dyspnea and lipothymia. The electrocardiogram showed normal sinus rhythm with ventricular pacing. Cardiac implantable electronic device interrogation data did not report any arrhythmic events. Orthostatic hypotension was evidenced on physical examination and attributed to the patient's antihypertensive medications. FDG-PET/CT (Figure 4.A) was repeated to exclude reactivation of sarcoidosis. Pathological FDG uptake remained absent within the myocardium and intrathoracic LN. Multiple ground glass opacities and reticulations appeared within both lung fields (Figures 4.B and 4.C) associated with areas of intense FDG uptake (SUVmax=8.1) (Figures 4.D and 4.E). Differential diagnosis included PS, infectious disease, and MtxIP. Cultures obtained from bronchoalveolar lavage were negative. MtxIP was deemed more likely, but PS could not be completely excluded. MTX was discontinued while oral prednisone was maintained at the same dose of 50 mg per day. Dosage of the patient's antihypertensive agents was reduced.

The patient's dyspnea improved and lipothymia did not recur. Follow-up FDG-PET/CT (Figure 5.A) was repeated two months following MTX discontinuation. The previously noted pulmonary lesions improved greatly both radiologically and metabolically (Figure 5.B and 5.C). Remaining lesions consisted mostly of fibrotic changes and were associated with absent or low FDG uptake (SUVmax=3.4). Pathological FDG uptake remained absent within the myocardium and intrathoracic LN. MtxIP was retained as the final diagnosis.

Discussion

MTX is an antimetabolite with proven benefits as an anti-inflammatory agent in various inflammatory conditions including sarcoidosis, inflammatory bowel diseases and rheumatoid arthritis (3). MTX can result in several manifestations of lung disease, including pneumonitis, pulmonary infection, and pulmonary lymphoproliferative disease. Pneumonitis is a serious complication of MTX treatment with a reported incidence of 3.3-5.5% (4,5). As eosinophils are frequently found within the lung interstitium, it is thought to be a hypersensitivity reaction (6). MtxIP typically presents subacutely with progressive dyspnea, cough and fever (4,7). Importantly, its incidence appears to have no correlation with the duration of therapy or total cumulative dose (8). While most patients recover after withdrawal of MTX alongside corticosteroid administration, irreversible interstitial pneumonia and subsequent death have been reported (9). Radiological features are variable and include diffuse parenchymal opacification, reticular opacities, centrilobular nodules and most commonly a non-specific interstitial pneumonia pattern (8,10). Hilar lymphadenopathy and pleural effusions have also been reported (10,11). To the best of our knowledge, this is the first case of MtxIP documented by FDG-PET, demonstrating it to be an FDG avid disease process. It is important for physicians to recognize that not all foci of increased uptake in a patient with known sarcoidosis is related to this pathology. Although PS may present similarly both radiologically and metabolically, differentiation of both entities requires a thorough clinical history and careful review of previous imaging studies (12,13). As management of MtxIP and PS differ significantly, appropriate and timely diagnosis may have prognostic implications.

Conclusion

To our knowledge, this is the first literature case report of MtxIP documented by FDG-PET. Clinicians should be aware of this entity in sarcoidosis patients treated with MTX. Given the scarcity of data, additional studies are required to establish patterns of FDG uptake in MtxIP.

Acknowledgements: None

Figures

Figure 1.

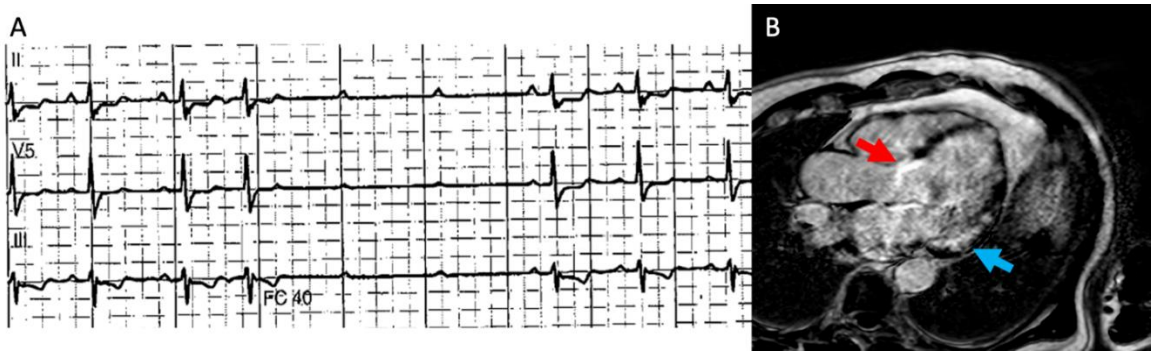

(**A**) Rhythm strip showing advanced atrioventricular block. (**B**) Cardiovascular magnetic resonance evidenced subendocardial late gadolinium enhancement within the basal interventricular septum (red arrow) and laterobasal wall (blue arrow) without increased T2-weighted signal.

Figure 2.

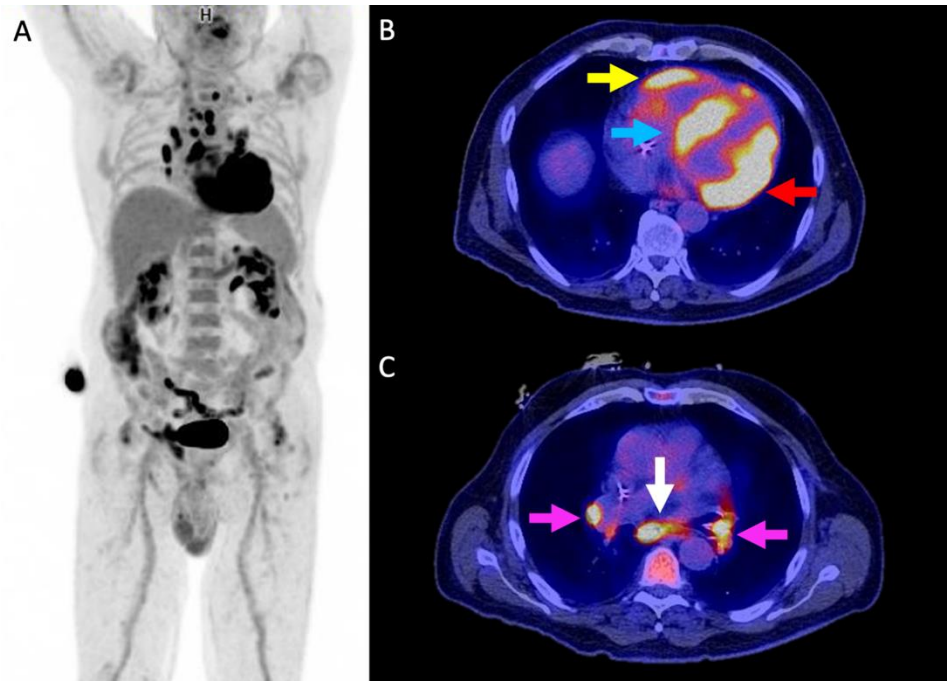

(**A**) Whole body FDG-PET/CT performed following myocardial suppression protocol (24h high-fat, low-carbohydrate diet, 12h fasting, intravenous heparin). (**B**) Intense patchy FDG uptake (SUV_{max}=15.4) was present within the myocardium at the levels of the left ventricular free wall (red arrow), interventricular septum (blue arrow) and right ventricle (yellow arrow). (**C**) Increased FDG uptake (SUV_{max}=14.9) was present within multiple intrathoracic LN, notably in the hilar (pink arrows) and subcarinal (white arrow) regions.

Figure 3.

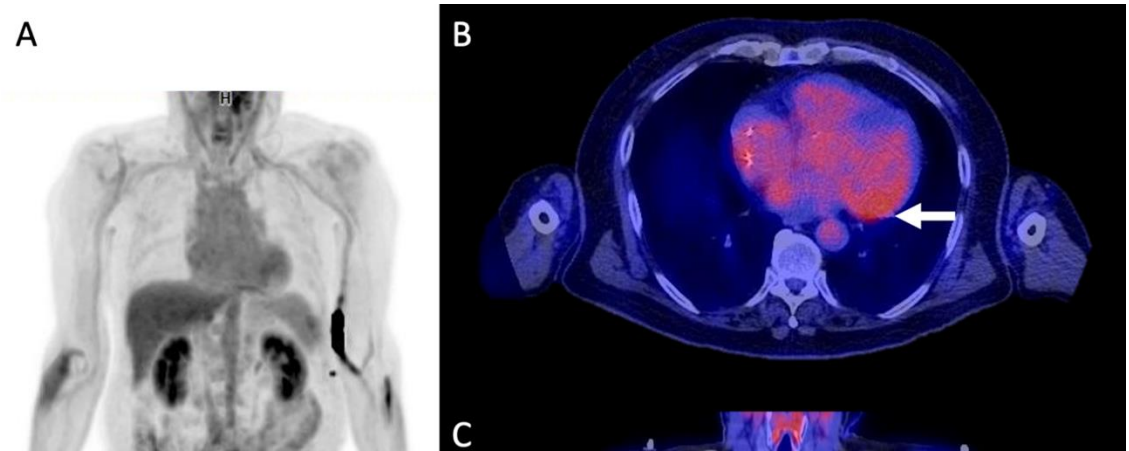

(**A**) Follow-up whole body FDG-PET/CT was performed following myocardial suppression protocol. (**B**) Overall, there was complete resolution of the multiple foci of intense FDG uptake in the myocardium with the exception of a low-grade area of uptake (SUV_{max}=3.5) within the basal anterolateral segment (white arrow), representing non-specific activity probably related to sub-optimal suppression. (**C**) Uptake within intrathoracic LN also completely resolved.

Figure 4.

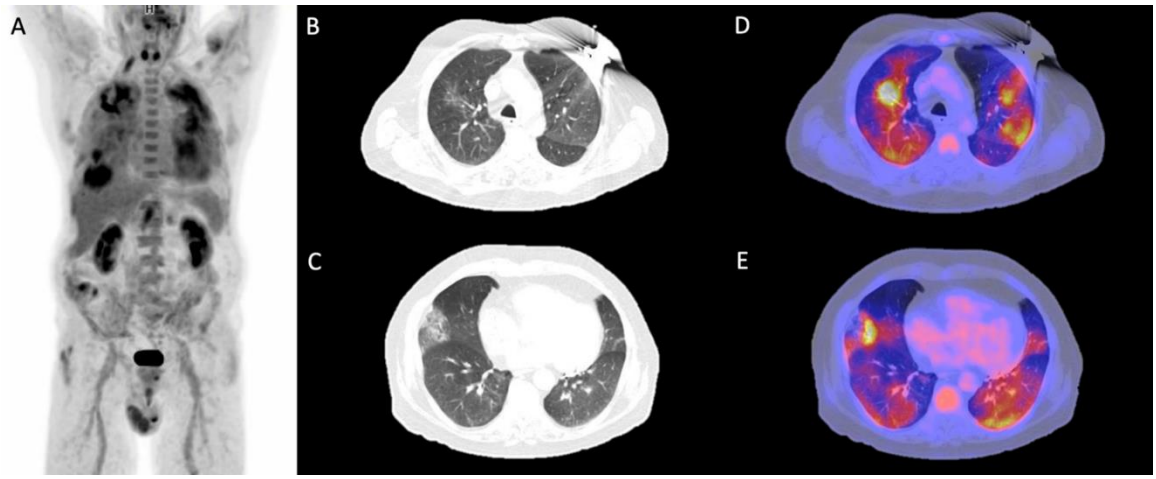

(**A**) Repeat FDG-PET/CT was performed following myocardial suppression protocol to exclude reactivation of CS. (**B, C**) Chest CT axial images showed multiple ground glass opacities and

reticulations within both lungs. (**D, E**) These changes were associated with intense hypermetabolism on FDG-PET/CT images (SUV_{max}=8.1).

Figure 5.

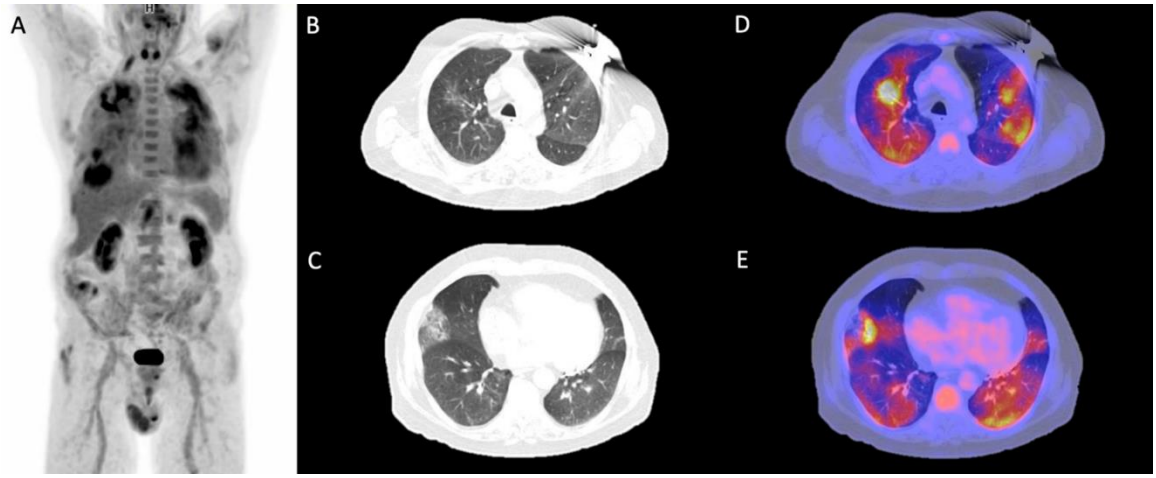

FDG-PET/CT (**A**) with myocardial suppression protocol was repeated two months following MTX discontinuation. (**B, C**) Fibrotic changes were seen within both lung fields and were associated with absent or low FDG uptake (SUVmax=3.4) (white arrows).

References

1. Terasaki F, Azuma A, Anzai T, et al. JCS 2016 Guideline on Diagnosis and Treatment of Cardiac Sarcoidosis ― Digest Version ―. Circulation Journal. 2019;83:2329-2388.

2. Birnie DH, Sauer WH, Bogun F, et al. HRS expert consensus statement on the diagnosis and management of arrhythmias associated with cardiac sarcoidosis. Heart Rhythm. 2014;11:1305–1323.

3. Imokawa S, Colby TV, Leslie KO, Helmers RA. Methotrexate pneumonitis: review of the literature and histopathological findings in nine patients. European Respiratory Journal. 2000;15:373-381.

4. Arakawa H, Yamasaki M, Kurihara Y, Yamada H, Nakajima Y. Methotrexate-Induced Pulmonary Injury: Serial CT findings. Journal of Thoracic Imaging. 2003;18:231-236.

5. Gispen JG, Alarcón GS, Johnson JJ, Acton RT, Barger BO, Koopman WJ. Toxicity of methotrexate in rheumatoid arthritis. J Rheumatol. 1987;14:74-79.

6. Smith GJ. The histopathology of pulmonary reactions to drugs. Clin Chest Med. 1990;11:95-117.

7. Cottin V, Bendstrup E, Bonniaud P, et al. The case of methotrexate and the lung: Dr Jekyll and Mr Hyde. European Respiratory Journal. 2021;57.

8. Rossi SE, Erasmus JJ, McAdams HP, Sporn TA, Goodman PC. Pulmonary Drug Toxicity: Radiologic and Pathologic Manifestations. RadioGraphics. 2000;20:1245-1259.

9. Hilliquin P, Renoux M, Perrot S, Puéchal X, Menkès CJ. Occurrence of pulmonary complications during methotrexate therapy in rheumatoid arthritis. Br J Rheumatol. 1996;35:441-445.

10. Kremer JM, Alarcón GS, Weinblatt ME, et al. Clinical, laboratory, radiographic, and histopathologic features of methotrexate-associated lung injury in patients with rheumatoid arthritis. A multicenter study with literature review. Arthritis & Rheumatism. 1997;40:1829-1837.

11. St Clair EW, Rice JR, Snyderman R. Pneumonitis Complicating Low-Dose Methotrexate Therapy in Rheumatoid Arthritis. Archives of Internal Medicine. 1985;145:2035-2038.

12. Criado E, Sánchez M, Ramírez J, et al. Pulmonary Sarcoidosis: Typical and Atypical Manifestations at High-Resolution CT with Pathologic Correlation1. RadioGraphics. October 2010.

13. Keijsers RGM, van den Heuvel DAF, Grutters JC. Imaging the inflammatory activity of sarcoidosis. Eur Respir J. 2013;41:743-751.

008- **Charles Intenzo**

Relationship between Radioiodine dosage and incidence of radiation gastritis in patients with well-differentiated thyroid cancer

Objectives: Radiation gastritis, namely nausea with or without vomiting, is a potential side effect in patients undergoing I-131 therapy for well-differentiated thyroid cancer (WDTC). Our goal was to determine if the likelihood of radiation gastritis (RG) is dose-related.

Methods: Over a 5-year period, at the time of the 1-week post-ablation whole body I-131 scan, patients were questioned regarding gastritis-related symptoms. The patients were divided into 3 groups according to the I-131 dosage, namely 100, 150, and 200 mCi, respectively.

Results:

I-131 dosage (mCi)	Incidence of RG symptoms (%)
100	66
150	71
200	75

There was no significant difference (p-value of 0.83) in the incidence of RG among the 3 different I-131 dosages dispensed.

Conclusion: For the patients with WDTC undergoing I-131 ablation, there is no direct relationship between the dosage dispensed in the range of 100 to 200 mCi, and the likelihood of developing radiation-induced gastritis.

009- **Anna Hwang**

Objective: To investigate quantitative features that can be extracted from 18-FDG PET/CT and correlated to TNM staging in patients with stage II/III breast cancer.

Methods: A systematic search was conducted using MEDLINE up until February 25, 2022, with keywords such as “breast neoplasms”, “PET/CT”, “radiomics”, “texture”, and “metabolic parameters”. After abstract screening (n = 578, two reviewers) and full-text screening (n = 135), 16 articles were included. These studies included only stage II/III breast cancer patients and utilized traditional semiquantitative and/or radiomic features.

Results: Eligible studies (2011-2021) included prospective (8/16) and retrospective (3/16) cohort studies, and ancillary analyses on prospective data (5/16). Both single-center (9/16) and multi-centric studies (7/16) were found (median sample size: 89 patients, range: 36 -214). Reported features included standardized uptake value (SUV), metabolic tumor volume (MTV), total lesion glycolysis (TLG), and higher-order/textural features. Regarding maximum SUV of the primary breast tumour, 8/11 studies reported no association with T or N stage, whereas 2/11 reported a weak association with T stage ($r = 0.45$ and 0.46, $p<0.008$). Regarding maximum SUV of lymph nodes, 5/6 studies found that higher SUV was associated with lymph node metastases (median SUV of metastatic vs. benign nodes: 5.45 vs. 2.79, $p<0.005$). Regarding MTV and TLG, 3/4 studies found a positive association with higher T stage ($p<0.01$). Four studies extracted textural/higher-order features. Of these, 3 studies reported association of T stage with selected textural PET features (homogeneity, entropy, contrast, or energy, $p<0.02$). Only one study extracted CT features, but no association was found with T or N stage.

Conclusions: Metabolic and textural features show modest association with clinical T/N stages in stage II/III breast cancer. Current research in this field is limited to studies using small datasets, with few studies investigating higher-order/textural features or radiomics quality scoring (RQS).

010- **Fahad Al-Lhedan**

Female Neonate Breasts Tissue Tc-99m Pertechnetate Uptake

Fahad Al-Lhedan and Ahmad Al-Faleh
King Abdullah bin Abdulaziz University Hospital, Riyadh, Saudi Arabia

Abstract

This is an unusually encountered imaging finding on tc-99m pertechnetate thyroid scintigraphy for a female neonate. The study goal is further assessment of thyroid function test derangement that was identified in the routine well baby clinic screening. Neonatal breasts focal symmetrical tc-99m pertechnetate uptake was incidentally depicted. Tc-99m pertechnetate cellular uptake depends on the transmembrane sodium-iodide symporter mechanism and this is normally present in breast tissues. Maternal lactogenic hormones transplacental transportation leads to enhancement of the transmembrane sodium-iodide symporter mechanism (1, 2, 3). This transplacental hormonal transportation with resultant transmembrane sodium-iodide symporter mechanism enhancement are the reasons behind we have surprisingly seen in this thyroid scan.

Introduction

Tc-99m pertechnetate ($Na^{+}\ ^{99m}Tc\ O_4^-$) is one of the technetium radiopharmaceuticals, which can be used for thyroid imaging, parathyroid subtraction technique, Meckel's diverticulum diagnosis and testicular scintigraphy. Tc-99m pertechnetate has a photon energy of 140 keV and a physical half-life of 6 hours. Stomach, thyroid and salivary glands and testicles reveal normal physiological tc-99m pertechnetate uptake while its excretion is via genitourinary and gastrointestinal tracts.

Case presentation

This is a female neonate who was found to have a significantly increased TSH level measuring 7.684 uIU/mL along with high T4 value, which measures 25.3 pmol/L in her routine well baby clinic laboratory investigations.

On physical examination: the patient was well, active and alert; she was not pale, jaundiced or cyanosed, vitally stable with no dysmorphic features and the systemic evaluation was unremarkable.

Thyroid gland ultrasound scanning was performed demonstrating no gross abnormality. Thyroid gland scintigraphy utilizing tc-99m pertechnetate was done showing normal thyroid gland location which has bilobed butterfly configuration displaying homogenous activity and the thyroid gland uptake was within normal limits. Normal physiological activity was noted in the stomach and salivary glands as well. However, there was unexpected breasts focal symmetrical tc-99m pertechnetate uptake.

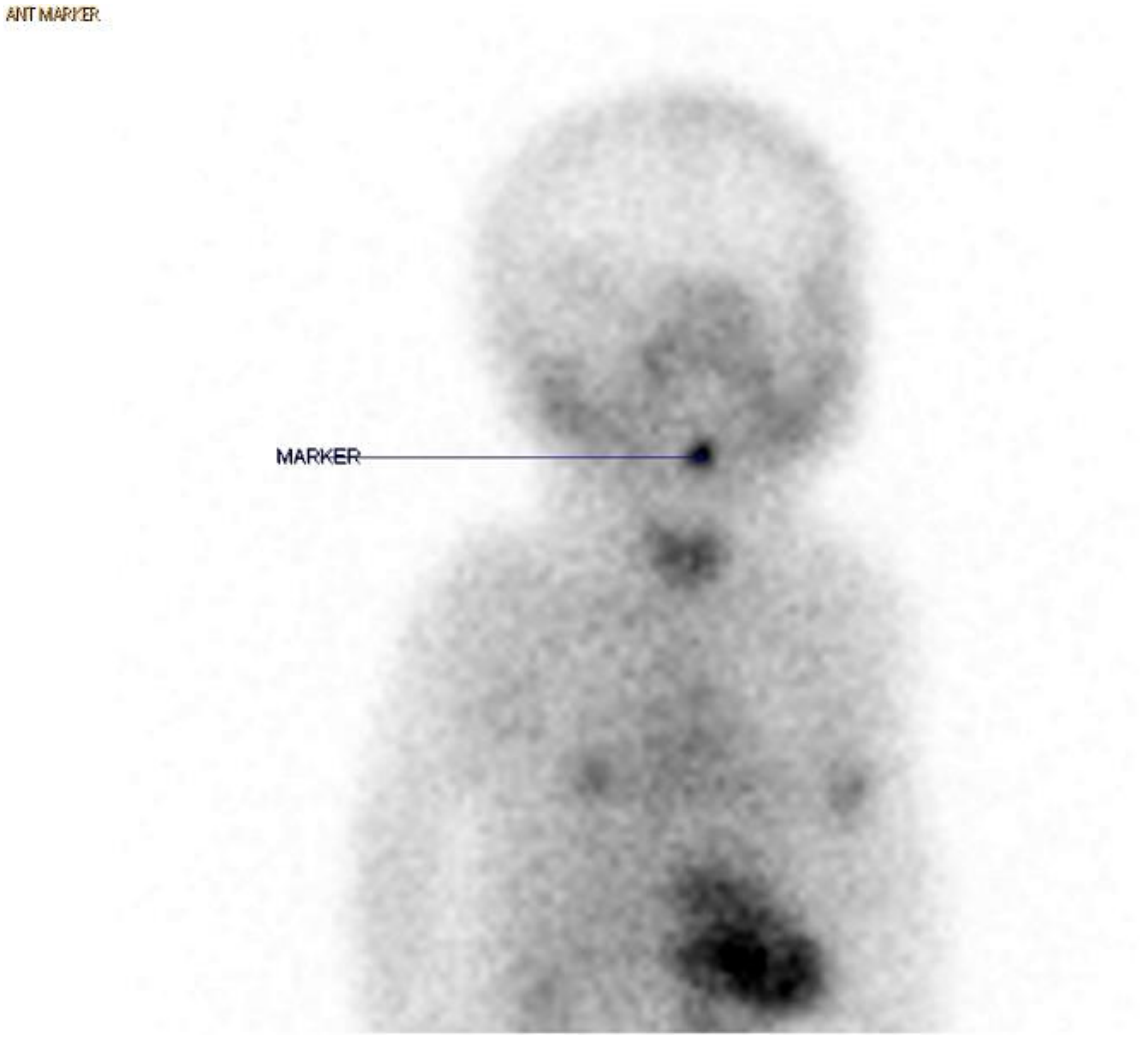

Tc-99m pertechnetate thyroid scan: normal thyroid gland uptake. Normal physiological gastric and salivary gland activity. Incidental finding of bilateral breast focal symmetrical pertechnetate uptake.

Discussion

Pertechnetate anion uptake in breast epithelial cells is mediated by transmembrane sodium-iodide symporter that is normally present in these tissues (4, 5). Many in vitro and in vivo studies have shown that lactogenic hormones such as, prolactin, estrogen and oxytocin do stimulate functional mammary tissues transmembrane sodium-iodide symporter expression (1, 4). Breast epithelial cells transmembrane sodium-iodide symporter mechanism was enhanced in this neonate secondary to transportation of the aforementioned maternal lactogenic hormones through the placenta (1). Subsequently, neonatal breast tissues displayed bilateral focal symmetrical tc-99m pertechnetate uptake on the thyroid scintigraphy. This is the only

reasonable explanation for this unusual finding and many cases were reported in the literature previously with the same observation confirming this theory.

Conclusion

Female neonate breasts tc-99m pertechnetate uptake is uncommonly seen scintigraphically and this is attributed to breast epithelial cells transmembrane sodium-iodide symporter mechanism enhancement, which resulted from transplacental maternal lactogenic hormones stimulation. This phenomenon should be kept in mind in order not to misinterpret this normal physiologically present imaging finding.

Conflicts of Interest

The authors declare that there are no conflicts of interest regarding publication of this paper.

References

[1] Shankaramurthy Gayana, Anish Bhattacharya, Koramadai Karuppusamy Kamaleshwaran, and Bhagwant Rai Mittal, Unilateral Breast Uptake of Tc-99m Pertechnetate in a Patient with Cold Nodule of the Thyroid, World J Nucl Med. 2012 May-Aug; 11(2): 79–80.

[2] Sachin Jain, Punit Sharma, Anirban Mukherjee, Chandrasekhar Bal, Rakesh Kumar, "Witch's milk" and 99mTc-pertechnetate uptake in neonatal breast tissue: an uncommon but not unexpected finding, Clinical Nuclear Medicine, 2013 Jul;38(7):586-7.

[3] Sonal Rakshpaul，Gaurav Malhotra，Sudha C Rao，Raj Narwade, Alpana Utture, Ramesh V Asopa, Bilateral Breast Uptake of 99mTc-Pertechnetate in a Neonate With Congenital Hypothyroidism, Clinical Nuclear Medicine, 2020 May;45(5):412-413.

[4] Ekaterina Tiktinsky, MD, Tifha Horne, MD, Svetlana Agranovich, MD, and Sophie Landsberg, MD, Unilateral Tc-99m Pertechnetate Breast Uptake: Is it Always Benign?, Clinical Nuclear Medicine, October 200732(9):735-6.

[5] CHONG G. CHEW, M.B.B.S., F.R.A.C.P., AND PAUL SOTIROPOULOS, B. Medical Radiation, Uptake of Tc-99m Pertechnetate By Lactating Breasts During a Thyroid Scan in a Postpartum Patient, Clinical Nuclear Medicine, Volume 28, Number 5, pp 441–442.

011- **Charles Intenzo**

The Role of Heat-denatured Red Blood Cell SPECT/CT Imaging of Ectopic Spleen Detection

Objectives: The presence of ectopic splenic tissue is sometimes an imaging challenge in anatomic imaging, such as CT or MRI. This atlas presentation demonstrates our experience in using Tc99m pertechnetate labelled to red blood cells (RBC) whose structure is altered by high-temperature incubation, which enhances trapping by any splenic tissue.

Methods: All patients referred for splenic imaging underwent SPECT/CT fusion imaging of the abdomen and pelvis at one hour after injection of the heat-denatured Tc99m-labelled RBC's. Indications for the studies were either s/p splenectomy (looking for leftover splenules) or to rule out splenic tissue versus mass lesion within the pancreas seen on MRI or CT.

Results: Heat-denatured RBC imaging via SPECT/CT correctly identified the presence or absence of all splenic tissue, which appeared very prominently in the images.

Conclusion: SPECT/CT imaging using heat-denatured RBC's is an optimum modality for the detection of ectopic splenic tissue.

012-

The Role of Cu-64-Dotatate PET/CT in the Workup of Brain Meningioma

Objectives: As a somatostatin receptor-positive tumor, brain meningiomas can be imaged by either In-111-pentetreotide (Octreoscan) or by PET agents, such as Ga-68-dotatate or Cu-64-dotatate. The PET agents are more sensitive given the superior spatial resolution. This atlas presentation demonstrates our experience in using Cu-64-dotatate to detect the tumor burden in patients with meningioma of the brain.

Methods: In select cases, patients with meningiomas are referred for dotatate imaging for guiding stereotactic radiosurgery. PET/CT brain imaging is performed at 1 hour after the injection of Cu-64-dotatate.

Results: The images detected both the extent and number of the meningiomas in the patients referred to us.

Conclusion: Cu-64-dotatate PET/CT is useful for targeting viable tumors in patients with brain meningiomas prior to stereotactic radiosurgery.

013- **Jessica Elise Kuizon**

The role of radioactive iodine therapy as adjunctive treatment in papillary thyroid microcarcinoma: A meta- analysis

Background. The controversy surrounding the optimal management for papillary thyroid microcarcinoma to this day still continues. The appropriateness of radioactive I-131 ablation, specifically in low and intermediate risk patients, remains to be a topic of debate among clinicians with most guidelines recommending against routine remnant ablation. With the recent increase in the incidence of papillary thyroid microcarcinoma globally, it becomes all the more important to settle this issue. This study aims to assess whether RAI ablation done post-operatively reduces the recurrence of papillary microcarcinoma in patients categorized as low to intermediate risk.

Methods. A comprehensive literature search of PubMed, Cochrane library, Medline, Embase, and Google Scholar for studies comparing the recurrence rate of papillary thyroid microcarcinoma between patients treated with surgery followed by RAI versus surgery alone was done according to the PRISMA guidelines. Studies including patients who underwent total or sub-total thyroidectomy with or without RAI ablation were included, regardless of the length of follow-up. The meta-analysis was then performed using review manager (Revman) version 5.4.

Results. A total of 11 studies, which included 5167 eligible patients, were reviewed and assessed. The rate of any site recurrence (i.e. biochemical and/or structural) for patients treated with surgery followed by RAI was lower than those treated with surgery alone (3.0% vs. 12.7%, RR = 0.19, $p < 0.00001$). Recurrence with structural evidence was also lower in patients treated with RAI compared to those treated with surgery alone (1.9% vs 4.7%, RR = 0.36, $p = 0.0007$).

Conclusion. Radioactive iodine remnant ablation after sub-total or total surgery decreases the rate of recurrence in low to intermediate risk PTMC patients.

014- **Amir Jabbarpour**

Automatic Perfusion Defect Detection in Lung Scintigraphy using Anomaly Detection with Convolutional Auto-Encoder

Amir Jabbarpour, Siraj Ghassel, Eric Moulton, Jochen lang, Ran Klein

Objectives:

Ventilation-perfusion (V/Q) scintigraphy has a major role to play in the diagnosis of pulmonary embolism (PE). The hallmark signature of PE is a V/Q mismatch corresponding to a region of the lung that is under-perfused with preserved ventilation. The objective of this study was to apply techniques in artificial intelligence (AI) and anomaly detection to automatically highlight areas of abnormal perfusion to facilitate image interpretation and detect abnormal V/Q studies.

Methods:

We retrospectively included 99mTc MAA planar perfusion images of 707 patients from The Ottawa Hospital who underwent V/Q scans for suspicion or follow-up of PE between June 2019 and February 2023. These data were acquired until a total of 600K counts were recorded in 6 projections. Images were translated to the center of the lungs and were then normalized in intensity. To perform anomaly detection, we built and trained a convolutional neural network auto-encoder (AE) on all projections of perfusion images for studies classified as “Normal” probability of PE according to the modified PIOPED criteria (N=578/707, 82%). The AE was trained using a mean absolute error (MSE) loss function and 80% of patients and validated on 20%. To highlight areas of abnormal perfusion, we passed a subset of abnormal perfusion studies (Intermediate and High PIOPED probability) through the AE and computed a reconstruction error image.

Results:

Qualitatively, the AE is able to localize segmental and sub-segmental perfusion defects in patients with confirmed PE and not introduce false positives on normal cases.

Conclusion:

The proposed AE model shows promise for localization of perfusion defects, automatic detection of abnormal cases, and potentially lung function quantification for other indications.

015- Siraj Ghassel

Evaluating the Effect of Resizing on Scintigraphic Images: An Image Similarity Analysis

Objective: To determine a resizing method that preserves count statistics and noise characteristics of scintigraphic images.

Methods: A phantom emulating a pulmonary ventilation-perfusion (V/Q) scintigraphy exam was used to acquire images at different common spatial grids, namely 256x256, 128x128, and 64x64. 779MBq of Technetium-99m (Tc-99m)-pertechnetate was administered as in a clinical V/Q scan. To reconstruct planar images at various count levels, we performed dynamic acquisitions comprised of 100 frames for 1 second each, resulting in 11 kcnts/image for a total of 1.1Mcnts. We derived image similarity reference curves as a function of count level by calculating the SSIM, PSNR, and MSE between two independent images acquired at the same spatial resolution by random shuffling and summing of the dynamic acquisitions. Upsampling methods consisted of linear interpolation with and without Poisson resampling to correct count statistics. Downsampling methods consisted of linear interpolation or sliding window summation. Image similarity metrics were then computed between resized images and count-matched images of the target resolution. Image similarity curves of the upsamling/downsampling experiments were compared to the reference similarity curves of the target resolution to determine which one overlay most with the reference curves.

Results: Upsampling with naïve linear interpolation yielded image similarity curves that deviated significantly from the reference curves. Following Poisson resampling correction, the similarity curves realigned with the reference curves for all projections, count levels, and spatial resolutions. For downsampling, linear interpolation and sliding window summation methods yielded comparable similarity curves as the reference curves when downsampling by a factor of two. However, for larger resizing factors, only block summed pooling produced excellent agreement with reference curves for all projections, count levels, and spatial resolutions.

Conclusion: Upsampling by linear interpolation and Poisson resampling correction and downsampling with sliding window summation yield more realistic scintigraphic images than resizing by linear interpolation alone.

016- **Patrick Causey**

P.W. Causey, B.A. Tamboline, M. Wong, A. Lee, R.W. Riddoch

BWXT Medical Ltd.

Supporting Early Phase Clinical Trials with Scalable Production of ^{227}Ac-free Actinium-225 from a Radium Generator Constructed Following Proton Spallation of Natural Thorium

Objectives

High energy proton spallation of natural thorium targets affords scalable construction of high activity radium generators capable of regular, repeated production of actinium-225, devoid of the long-lived radioimpurity actinium-227 and other isotopes of concern. The goal was to efficiently isolate the desired radium isotope from a complex mixture comprising most elements from the periodic table. The unique process needed to be operator-friendly, robust, and repeatable at increasing scale. The developed processes have enabled the production of high quality Ac-225 meeting required product specifications to satisfy and surpass regulatory requirements as an Active Pharmaceutical Ingredient for early phase Targeted Alpha Therapy clinical trials.

Methods Used

Irradiation of thorium metal targets is performed at the Isotope Production Facility (IPF) using TRIUMF's 500 MeV cyclotron. Radiochemical processing is undertaken in dedicated hotcells in BWXT's Radiochemistry Annex, also situated at TRIUMF. Initial target digestion steps ensure access to all formed isotopes, along with the controlled removal of volatile radioimpurities. Following bulk thorium removal, isolation and radiochemical separation of desired radium is accomplished by chromatography, yielding a radium generator. Time for actinium-225 in-growth is allowed, in order to maximize operational performance and product yields, before product dispensing and Quality Control release of the final product. All analytical methods have been validated, including radionuclidic purity, radiochemical purity, and a representative radiolabeling assay. BWXT Medical follows ICH Q7 Guidelines for production of Active Pharmaceutical Ingredients, and complies with regulatory bodies, include FDA, Health Canada and European Medicines Agency.

Results

In less than one calendar year, BWXT progressed from the project planning stage, through development, in order to qualify as a supplier for Ac-225 for a recently initiated clinical trial on Metastatic Castration-Resistant Prostate Cancer, sponsored by Bayer Pharmaceutical (EU CT Number 2022-502623-22-00). Key Project milestones and Development learning opportunities will be presented.

Conclusions

BWXT Medical is uniquely positioned to leverage the significant successes realized in our actinium from spallation project in order to ensure the scalable production of critical quantities of Ac-225 to support clinical trials.

017- **Mohsen Ansari**

Comparison of Spatial Normalization Strategies in Perfusion Scintigraphy for Patient-Specific Registration to a Bronchopulmonary Segment Atlas

Mohsen Ansari, Amir Jabbarpour, Eric Moulton, Jochen Lang, Ran Klein

Objectives:

To determine a spatial normalization strategy of perfusion scintigraphy images that reduces excessive distortions for registration to a Bronchopulmonary Segment Atlas (BSA) as a diagnostic aid for pulmonary embolism.

Methods:

Planar perfusion templates were created through iterative registration and averaging of patients with normal V/Q scans on which a BSA was manually drawn by a trained nuclear medicine physician.

For spatial normalization of perfusion scans to the templates, three strategies were explored: (1) naïve registration directly to the template, (2) cost function masking in which perfusion defects were contoured and excluded from the cost function calculation, and (3) pre-processing with an auto-encoder (AE) pre-trained on normal V/Q scans to automatically remove defects before registration.

We captured the effect of each registration strategy on distortions of perfusion defects through two metrics: (1) the log determinant of the Jacobian of the deformation field [log(det(J))] and (2) the perfusion defect mask size post-registration. To determine significant differences in the explored methods, we performed two repeated measures ANOVA analyses with each metric as a dependent variable and registration strategy as a within-subject factor.

Results:

The ANOVA revealed a significant difference between registration methods for metrics ($F=0.0007$, $p<0.001$). Post-hoc t-tests revealed that naïve registration resulted in more pronounced distortions, given by significantly smaller log(det(J)) values and smaller defect sizes with respect to lesion masking and AE pre-processing ($p<0.001$), which both yielded comparable degrees of distortions ($p>0.05$). Visually, cost function masking and AE pre-processing were robust to perfusion defects and thus similarly preserved the natural morphology of the bronchopulmonary segments when overlaid on patient images.

Conclusions:

Removing perfusion defects with an AE prior to spatial normalization is a fully automatic and reliable method to lessen undesirable distortions during the registration process and thus enable a more accurate overlay of a BSA to patient images.

018- **Wissam Mosleh**

Automated Segmentation of Left Ventricle Myocardium on ^{82}Rb PET

Wissam Mosleh, Ran Klein, Jochen Lang, Robert deKemp

Objective: This study aims to develop a convolutional neural network (CNN) for automatic LV segmentation.

Method: Myocardial Blood Flow (MBF) quantification with Cardiac Positron Emission Tomography (PET) is an important tool for the early diagnosis and prognosis of coronary artery disease (CAD). This is achieved by first performing automated PET segmentation of left ventricle (LV) myocardium; however, even with the most automated software available, manual correction is needed for 10-15% of scans which is not efficient. We started off by collecting the data comprised of Rubidium-82(^{82}Rb) static myocardial images at rest and stress states of 142 patients from two scanners (GE Discovery 600 and 690). Manual segmentations of the LV were performed with FlowQuant and ITK-Snap. Then, the dataset was split into training/validation/test sets with 60:20:20 ratio, where the training and validation sets were used in the training phase and the test set was used to evaluate the model's performance. In addition, a generator was developed to do on-the-fly rotations and translations for augmentation for the training images. A 3D UNet was trained using a Dice loss, also we used callbacks for early stopping whenever the validation loss no longer increased for 15 consecutive epochs.

Result: The UNet was trained with little overfitting and generalized well onto unseen test data.
The average ± SD dice score on the test set was 0.93 ± 0.03. Also, the comparison of the true and predicted LV volumes yielded a Pearson $r=0.96$ ($p<0.001$).

Conclusion: Our UNet can generate LV segmentations with high accuracy and may reduce the need for manual intervention and inter-operator variability for downstream processing of myocardial perfusion.

019- **Quinn de Bourbon**

Characterization of AI performance for lesion detection using synthetic lesions

Quinn de Bourbon, Ran Klein

Objective: To evaluate the feasibility of characterizing the limits of detection of lesion in FDG PET/CT by artificial intelligence using synthetic lesions as ground truth.

Methods: Raw FDG PET/CT (GE Discovery 710 scanner) was collected from our clinic, for patients reported free of lesions by physicians. An in-house developed Lesion Synthesis Toolbox (LST) software was used to manually define spherical, artificial lesions of known sizes (1-15 mm) and intensities (0.5-6 times liver activity) in anatomically realistic sites. Lesions were forward projected and added to the raw PET data before reconstruction using our clinical protocol (Q.Clear, beta=550). Lesions were also appended to the reconstructed CT images. PET/CT images with lesions were sent to two research teams developing AI for lesion detection. AI reported lesions were compared to ground truth data. AI lesions were labelled as detected if they were within 1 cm of a ground truth lesion. Ground truth lesions that were not within 1 cm of AI lesions were marked as missed. Detected and missed lesions were graphed by size vs intensity relative to the liver and by size vs contrast with background. We hypothesized that large, intense lesions would be detected with greater accuracy than small, faint lesions.

Results: 575 lesions were added to 116 simulations of 59 patients (average 2 simulations per patient, and 5 lesions per simulation). Detected vs missed lesions were better separated on graphs by size vs contrast than in graphs of size vs intensity. True positives were associated with larger size and higher intensity. The AIs differed in performance with method A reliably detecting smaller lesions with less false positives than method B.

Conclusion: Synthetic lesions are a useful tool for characterizing and comparing the performance of AI for lesion detection. Performance is better characterized in terms of lesion contrast than intensity.

020- **Siraj Ghassel**

Utilizing Conditional Generative Adversarial Networks (cGANs) for Artificial Count Enhancement of Lung Scintigraphic Images

Objective: To develop an image-to-image translation model capable of generating synthetic high-count lung scintigraphic images from low-count ones.

Methods: *Patients.* We retrospectively included 299 patients from The Ottawa Hospital who underwent V/Q scans for either acute diagnosis or chronic follow-up of pulmonary embolism (PE) between Sept 2019 and Mar 2022. *Image Acquisition.* Only perfusion images using 99m-Tc MAA were used in this study were recorded using a 256×256 matrix. We implemented Poisson resampling to generate synthetic images having a third of the reference high-count images. *Model training.* Training, validation, and test sets were constructed with an 80:10:10 split. We trained a cGAN on paired low and high-count images using a combination of L1, perceptual, and adversarial based losses to ensure both high-level feature similarity and pixel-level accuracy. Stopping criteria was determined by L1 loss on the validation set not improving for 10 epochs. *Model evaluation.* We calculated MSE, peak signal to noise ratio (PSNR), and structural similarity index measure (SSIM). Image similarity metrics were compared with paired t-tests.

Results: The cGAN was trained for 201 epochs and showed little overfitting, with a SSIM, PSNR, and MSE of XX, XX, and XX, respectively. By visual inspection, we show that subsegmental and segmental perfusion defects can still be discerned after enhancement and no new defects are introduced. From the low-count to synthetic high-count, the MSE changed by -5.39 ± 4.22 ($\times 10^{-4}$), PSNR by 2.53 ± 1.49, and SSIM 0.0582 ± 0.034 (all $p<0.001$), demonstrating that the synthetic high-count is closer to the high-count planar.

Conclusion: The proposed cGAN model appears to be promising for artificially enhancing counts to reduce scan acquisition times and to generate pseudo planar images from SPECT data.